Earth and Planetary Science Letters 472 (2017) 229–240

Contents lists available at ScienceDirect

Earth and Planetary Science Letters

www.elsevier.com/locate/epsl

Milankovitch cycles in an equatorial delta from the Miocene of Borneo

Nathan Marshall [a,*], Christian Zeeden [a,b], Frederik Hilgen [a], Wout Krijgsman [a]

[a] Utrecht University, Department of Earth Sciences, Budapestlaan 17, 3584 CD Utrecht, The Netherlands
[b] IMCCE, Observatoire de Paris, F-75014 Paris, France

ARTICLE INFO

Article history:
Received 21 May 2016
Received in revised form 6 April 2017
Accepted 10 April 2017
Available online 20 June 2017
Editor: H. Stoll

Keywords:
Milankovitch
Borneo
Indonesia
Indonesian throughflow
Miocene
cyclostratigraphy

ABSTRACT

The factors controlling sedimentary cyclicity in deltaic systems are a subject of intense debate, and more research, in different deltaic environments and time periods, is needed to better understand the possible mechanisms. Offshore and Pleistocene case studies are more common than proximal and more ancient, greenhouse-climate examples. Furthermore, many studies lack a (statistical) cyclostratigraphic element. The paleo-Mahakam delta of Eastern Kalimantan, Borneo developed during the globally warm middle Miocene, in an equatorial setting, making it of interest to comprehend cyclic sedimentation in a period of warmer yet rapidly changing climate. In this study, statistical analysis of lithological changes shows that regular sandstone/shale alternations occur in a distinct pattern of cycles with thicknesses of ~90, ~30, and ~17 m. Using independent dating, these thicknesses translate into periods of about 100, 40, and 20 kyr, matching the known periods of Earth's orbital eccentricity, obliquity and precession. The obliquity dominance in the middle interval is markedly similar to that observed in the global marine isotope (benthic $\delta^{18}O$) and other cyclic proxy records for this time interval. Despite a mismatch in the number of 40 kyr cycles compared to the global record that can be plausibly linked to the major sea-level drop at ~13.8 Ma and facies shifts, it appears that the proximal setting of the paleo-Mahakam's sedimentation was dominantly controlled by allogenic orbital forcing, probably as a consequence of glacioeustasy. In particular, the observed obliquity dominance at paleo-equatorial latitudes, as seen in other records, highlights the dominance of orbital forcing, and potentially glacioeustatic sea level change, during this crucial period of warmer climate.

© 2017 Elsevier B.V. All rights reserved.

1. Introduction

While "deltaic cycle" has entered into common parlance in sedimentology textbooks, the cause of these is a topic of active debate (e.g. Coe et al., 2003; Nichols, 2009; Miall, 2014). Deltas are influenced by numerous mechanisms including inland precipitation change, geomorphic variation, sea-level fluctuation, and tectonic activity. Cyclically changing parameters of Earth's orbit, known as Milankovitch cycles, exercise a pervasive control on the planets climate and is influential on sedimentation (e.g. Hilgen et al., 2014 and references therein). However, other processes can cause repetitive sedimentary processes: for instance, research have shown that autogenic river fluctuations can also feed deltas in a cyclic fashion (Miall, 2014). Disentangling all possible local, regional and global influences on a river system is challenging to the point that deltas might be considered to be a poor setting for studying Milankovitch cyclicity (Miall, 2014). Nevertheless, several studies from the recent glacial period (i.e. Pleistocene) indicate that Milankovitch-controlled glacioeustatic sea-level fluctuations exerted a strong control on delta systems (e.g. Saller et al., 2004; Macklin et al., 2012; Peeters et al., 2014). Moreover, there are a growing number of examples of ancient fluvial/deltaic systems in non-Icehouse periods (e.g. Cretaceous, Eocene, etc.) in which an allogenic climatic control (either sea-level or rainfall) is invoked as a primary control on cyclic sedimentation (e.g. Kodama et al., 2010; Zhu et al., 2012; Abels et al., 2013). These warmer time periods are interesting to study because, in theory, eustatic sea-level fluctuations are less of a factor since glaciers were less prevalent. In the above listed examples, initial evidence for orbital forcing is based on calculated time-frequencies for sedimentary cycles that fall within the range of Milankovitch periodicities. Tectonically driven changes typically take place at rates that are an order of magnitude slower than Milankovitch frequencies and can be shown to be distinct from the otherwise more regularly occurring and higher frequency deltaic cycles (e.g. Miller et al., 2005; Zhu et al., 2012; Bowman and Johnson, 2014). High sediment supply generated by regional tectonic uplift of the headwaters can be a key factor in preserving Milankovitch cycles, as sediment loading at the margin

* Corresponding author.
E-mail addresses: N.T.Marshall@uu.nl (N. Marshall), Christian.Zeeden@obspm.fr (C. Zeeden), F.J.Hilgen@uu.nl (F. Hilgen), W.Krijgsman@uu.nl (W. Krijgsman).

http://dx.doi.org/10.1016/j.epsl.2017.04.015
0012-821X/© 2017 Elsevier B.V. All rights reserved.

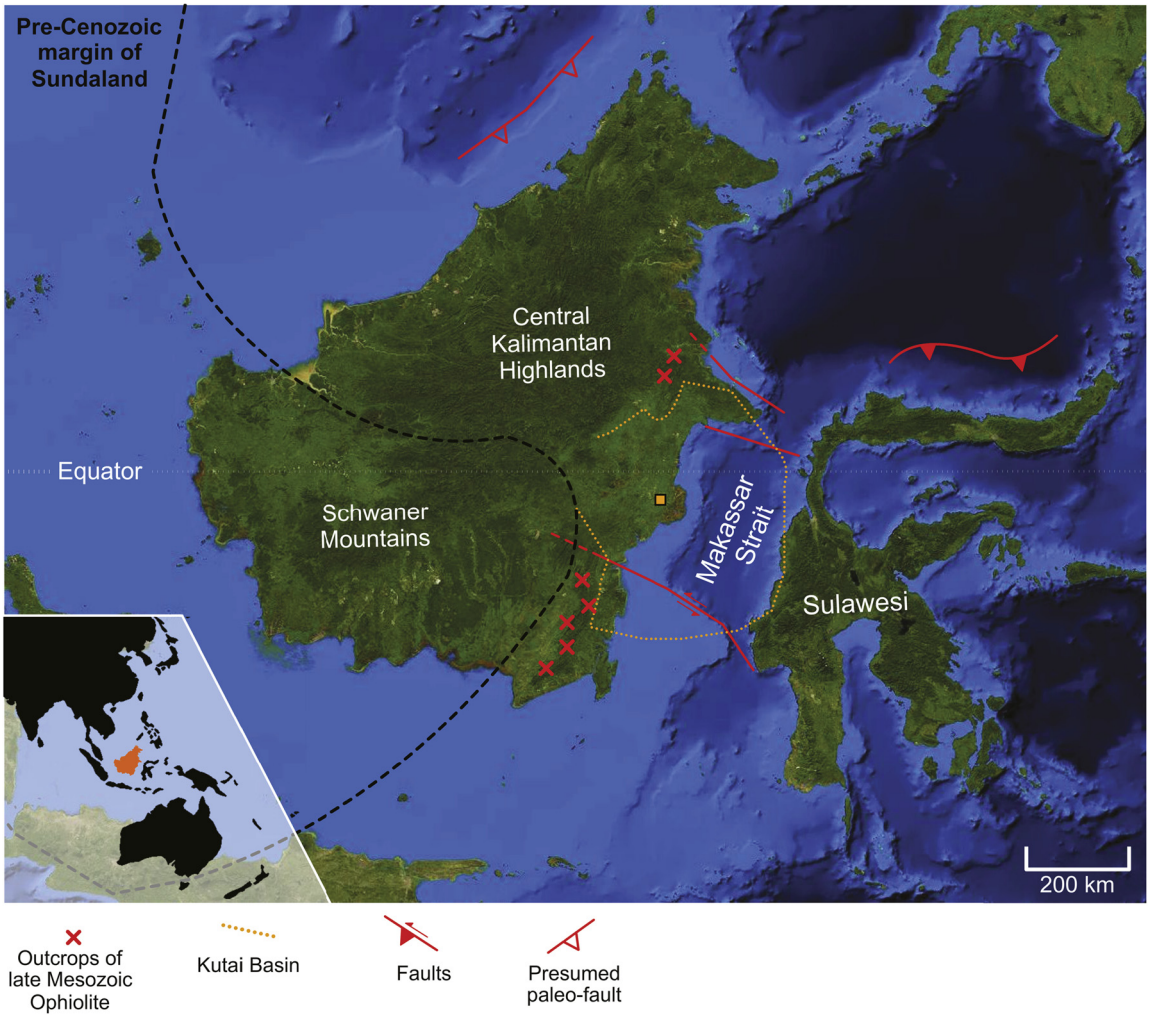

Fig. 1. Inset map highlights the location of Borneo within SE Asia (orange). Overview map sketch the key large-scale tectonic events of Borneo's history: the Mesozoic collision zone of SW Sulawesi (note location of ophiolite). In the Eocene, the Makassar Strait opened, initiating the Kutai Basin (orange dotted line). NE–SW normal faults run along the Makassar coast of Borneo through the Kutai Basin, from this rifting event. Inferred subduction from the opening South China Sea uplifted the Central Kalimantan Highlands, which are the primary source of sediment feeding the Kutai Basin. Study location is centered on the Miocene depocenter of the basin, just inland of the current Mahakam Delta (orange square). (For interpretation of the references to color in this figure legend, the reader is referred to the web version of this article.)

augments basin flexure and allows for a more continuous sedimentary record in the delta (e.g. Bowman and Johnson, 2014). Support for allogenic cycles is further bolstered if statistical analysis can confirm cycle periodicities and that those cycles match known orbital periods (e.g. precession, obliquity, etc.) of that time period (e.g. Abels et al., 2013; Meyers and Sageman, 2007).

Here, we present a relatively long (650 m) deltaic record from the middle Miocene (Langhian, approx. 15–14 Ma) of the Kutai Basin in East Kalimantan (Borneo, Indonesia; Figs. 1 and 2). The (semi-)continuous record afforded by high sedimentation rates offers a unique opportunity to investigate the possible causes of deltaic cyclicity, both during a dynamic period of climate change and in an equatorial system hypothetically less influenced by glacioeustatic effects. Importantly, this section contains a notable ancient reef system that has been used as a biodiversity milestone for understanding the growth of the current biodiversity hotspot in Indonesia (e.g. Renema et al., 2008; Santodomingo et al., 2016). By better understanding the controlling forces of sedimentation, a better picture can be gleaned as to what conditions fueled intermittent patch-reef formation that supported biodiversity proliferation in the region. This succession was initially studied for an integrated bio- and magnetostratigraphy campaign that places the succession during the key time period of transition from a Greenhouse climate, at around 15 Ma, to the significant cooling event at ~14 Ma (Marshall et al., 2015). During this previous study, it was observed that the succession appears to be remarkably cyclic (Fig. 3). The aim of this study is to statistically test if lithologic alterations are regular and if allogenic climate forces can be a possible mechanism. We find that sandstone-shale alterations are statistically cyclic and moreover; calculated time-periodicities based on independent dating, match well to the Milankovitch cycles found in other climate records of the same age.

2. Time interval and geological setting

2.1. Middle Miocene

The middle Miocene (circa 16–12 Ma) is an important period for the understanding of Earth's climate and the influence of orbital forcing on sedimentation. During this time, a major shift in Cenozoic climatic evolution occurred: global climate transitioned from Greenhouse to the current Icehouse. Following the climax of Neogene warmth at around 15 Ma, paleoclimate records indicate an overall cooling trend and significant short term variations in global temperature, glacial ice volume and sea-level (Flower and Kennett, 1994; Badger et al., 2013; Holbourn et al., 2013, 2015). At around 14 Ma, this cooling trend culminated in a large shift in $\delta^{18}O$ and $\delta^{13}C$ values evidencing a key cooling event accom-

panied by a major sea-level fall (40–70 m: John et al., 2011; De Boer et al., 2012; Holbourn et al., 2015). The end of the Miocene climatic optimum (MCO) corresponds with the substantial growth of the East Antarctic Ice Sheet (EAIS), initiation of glaciers in the Northern Hemisphere, and changes in ocean (especially meridional) circulation (De Boer et al., 2012; Badger et al., 2013; Holbourn et al., 2013). This crucial period of climate transition offers a distinct opportunity to explore the mechanisms of significant climate change and the interplay of the glaciers, climate, sea-level and ocean circulation. Currently, the interaction of processes that drove the middle Miocene climate transition remains poorly understood. One key hindrance is the scarcity of well-dated Miocene sedimentary records.

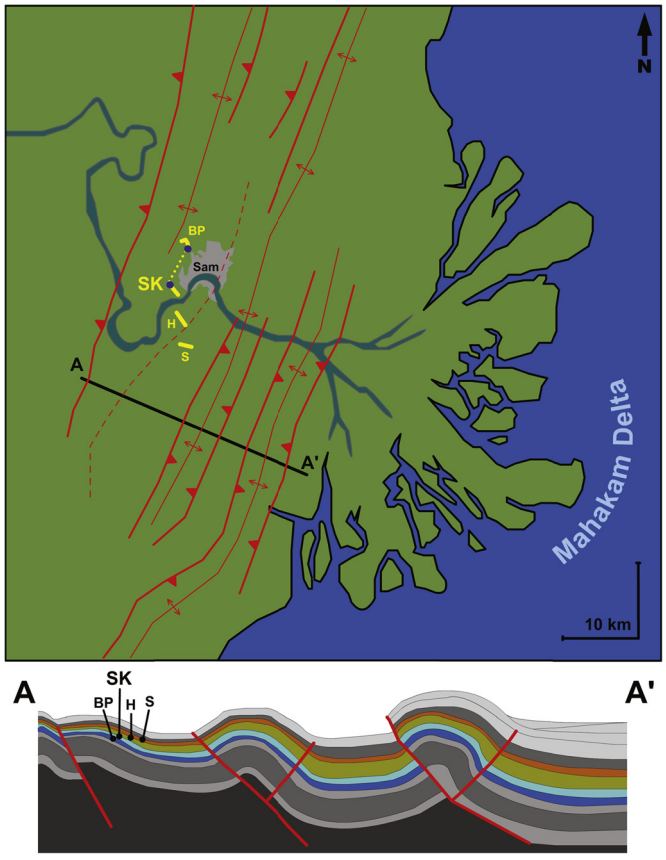

Fig. 2. Map of the Mahakam Delta and Samarinda region. The current structural features are presented based on McClay et al. (2000) and Cibaj (2013). Yellow lines highlight the exposures used for Magnetostratigraphy in Marshall et al. (2015), including SK = Sungai Kunjang, which is the focus of this study. Blue dot indicates the tie point of the Batu Putih. Cross-section A–A′ is redrawn from McClay et al. (2000), showing the location of the outcrops studied in Marshall et al. (2015) and this paper (SK). Colored strata are the age and environmental equivalents to the succession studied in Marshall et al. (2015). (For interpretation of the references to color in this figure legend, the reader is referred to the web version of this article.)

2.2. Kutai Basin

Presently, the Mahakam Delta feeds the Kutai Basin, which is the second largest and the deepest basin in Borneo. Development of the basin began in the Eocene, when southwestern Sulawesi rifted from Borneo, opening the Makassar Strait (Figs. 1 and 2). By the late Eocene, local depocenters, within the syn-rift half-grabens, merged into broader regional basins and formed the Kutai and other smaller basins along eastern Borneo (Fig. 1; Moss and Chambers, 1999; Hall and Nichols, 2002). During the Miocene, a profound increase in sediment supply occurred, caused by crustal thickening, uplift and volcanism within the Central Kalimantan Mountains (Hall and Nichols, 2002). Although debated, the best explanation for this sudden surge of uplift and sedimentation is from the underthrusting of the South China Sea floor under northwest Borneo (Fig. 1; Hall, 2009). Large amounts of sediment fed deltas that prograded rapidly away from the island. More than nine of the 14 km of Cenozoic sediment thickness in the Kutai Basin was added since the Early Miocene (Chambers and Daley, 1997; Hall and Nichols, 2002). The current Mahakam Delta is situated nearly in the center (just east) of the Miocene depocenter of the Kutai basin, indicating that when the river system migrated to this point in the Miocene its position seems to have stabilized at its current location so that sediment accumulation has been in the form of aggradational stacking and punctuations of progradation, with accommodation space generated by sediment-loading induced subsidence in addition to continued rift-related thermal subsidence (Saller et al., 2004; Cibaj et al., 2014). Initially, the sediment within the Kutai Basin appears to be from a volcanoclastic-recycled orogenic source and shifted to a cannibalized sedimentary source caused by basin inversion throughout the Miocene (Hall and Nichols, 2002).

Today, the Miocene succession of the Kutai Basin has been folded and faulted because of basin inversion. Seismic studies have demonstrated that the NNE–SSW-trending ridges of central–eastern Borneo are manifestations of tight linear anticlines and broad open synclines forming from reactivation of rifting-related faults (Fig. 2; Chambers and Daley, 1997). The dating of the earliest inversion event in the Kutai Basin is poorly controlled, in part because pre- and syn-inverted sedimentary rocks have been eroded, but probably occurred at least by the middle Miocene according

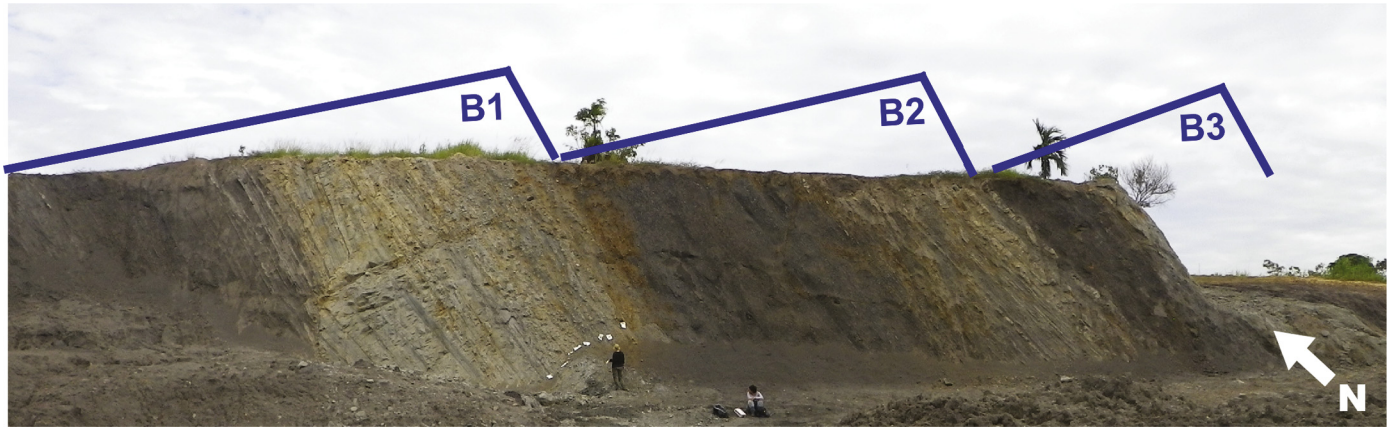

Fig. 3. Sungai Kunjang outcrop, between 140 m and 220 m stratigraphically. Observed shale/sandstone cycles are noted as presented in Fig. 4 and later figures. Note the two people (standing and sitting) for scale.

to Chambers and Daley (1997) and at approximately 14 Ma by McClay et al. (2000). Inversion started first in the west and propagated eastward. Thus, inversion in the field area occurred a bit later than this. Published local (Marshall et al., 2015) and regional basin studies (e.g. Morley et al., 2006) have shown that reworking in eastern Kutai Basin occurred in later time periods. This is illustrated by the common presence of robust NN4/NN5 (~18–13.5 Ma) calcareous nannofossils (i.e. *Sphenolithus heteromorphus*) in stratigraphically younger sediments containing other age-diagnostic fossil assemblages (particularly in situ larger benthic foraminifera) that point to a younger age (i.e. 12–11 Ma; see Marshall et al., 2015 for discussion).

The study area and the entire succession used for dating by Marshall et al. (2015) lies just east of the more structurally disturbed part of the basin (McClay et al., 2000; Cibaj, 2013). Fig. 2 provides a cross section proposed by McClay et al. (2000), which shows that the studied interval is east of the Separi/Taluang overthrusted anticline, within a broad and largely undisturbed syncline, which is confirmed by the stratigraphic correlation presented in Cibaj (2013).

2.3. Sungai Kunjang section

During the middle Miocene, the depocenter for the basin was around the city of Samarinda (Figs. 1 and 2). Urban development in this area has produced extensive exposures of middle Miocene sedimentary rocks including a 650 m thick section (Batu Putih–Sungai Kunjang: Marshall et al., 2015; S0.5172°, E117.1000°) covering the shelf to delta transition of the paleo-Mahakam River. A magneto-biostratigraphic study places this section within the time interval 15.5 to 13.5 Ma, corresponding to the Langhian (Fig. 4; Marshall et al., 2015). At that time, Borneo was close to its current equatorial position (e.g. Replumaz and Tapponnier, 2003; Hall, 2012).

The lower limey interval is interpreted as the turbid delta-front patch-reef known as Batu Putih ("Air Putih" in Wilson, 2005; Santodomingo et al., 2015). Directly above the patch-reefs are ~650 m of rhythmic alternations of shale and sandstone beds (Fig. 3). Decameter-scale sandstone intervals include packages of tightly stacked, coarsening up, of individual silt-to-sandstone beds. As noted in Cibaj (2009), many sandstone beds, particularly the coarsest, display sharp bases indicating erosion. The top of sandstone beds, before the start of shale dominated intervals, frequently have palm root traces, worm burrows and marginal marine fauna, such as echinoids. Shale intervals are often barren of fossils although occasional shallow marine fossil horizons are present directly following a sandstone interval and are more common below 250 m stratigraphically. Coal beds often have a sulfur crust on them indicating a marine influenced origin. Cibaj (2009, 2013) interprets the transition from shale to sandstone as a falling stage systems tract. In this way, sandstone beds represent a key period right after highstand when the ensuing lowering of sea level releases coarser sediment. Limestone and the shale occurring immediately above a sandstone dominated interval are interpreted to be a transgressive/highstand systems tract.

3. Methodology

3.1. Observed cycles

Careful examination of the sediments, paleobiology and depositional fabrics went into documenting the lithological log. Logging of the section was done at a sub-meter resolution in order to note subtle environmental features important for facies analysis and is presented in Cibaj (2009, 2013).

For this study, cyclic sedimentation here represents a series of coarsening upward packages. Each starts at the limestone or shale directly above a sandstone interval and ends at the top of the succeeding sandstone package, recording a change in grain size and facies boundaries. Observed cycles are noted with their height in meters (Fig. 4). Smaller, nested, cycles might also be present (for instance from 400–500 m; Fig. 4). A more detailed view of the stratigraphic column is provided in the supplementary materials for this paper.

3.2. Statistical analysis

3.2.1. Dataset

Beds are categorized as limestone, shale, siltstone (fine, medium, coarse) sandstone, conglomerate and coal. For statistical analysis, each of the lithologies was given a *lithology number value* (0–7) with higher values representing coarser grain-size and perhaps less marine influenced sedimentary environment. (#0) The patch-reefs are considered a sedimentation minimum since the carbonate factory (especially coralline) is typically hindered by high clastic input. (#1) Given the sulfur content and coal's typical presence in transgressive systems, coal is interpreted as a low energy environment associated with relative sea level rise (Diessel, 2006; Sykes and Cibaj, 2010). (#2–7) Sediments from clay to conglomerate are interpreted as progressively more proximal environments caused by relative sea level fall/progradation.

In this study, meter scale data resolution is used because field observation indicated that shale-sandstone alternation occurs at decameter scale and thus should be a suitable way to pick up possible cycles. At every meter on the lithological log, the lithology number value was recorded. 650 data points were generated for statistical analysis. Before further analysis these data were detrended by subtracting a taner low-pass filter (Taner, 1992; Meyers, 2014) with a cut-off frequency of 0.0045 and a roll-off rate of 200.

3.2.2. Time series analysis

Time series analysis is applied to the lithologic log, as demonstrated useful for cyclostratigraphy (e.g. Mitchell et al., 2008; Valero et al., 2015). Wavelet analysis (Grinsted et al., 2004) pictures the evolution of cyclicity with stratigraphy through the section (Fig. 2), and is often used to (a) depict the cyclic behavior of a dataset with stratigraphy and (b) check whether cyclic behavior changes in a dataset. Evolutive harmonic analysis (EHA; Thomson, 1982; Meyers, 2014) supplements the wavelet analysis, and represents a different technique to trace cyclic behavior through time. In contrast to wavelet analysis, EHA does not pick up signals representing solely amplitude modulations. Here a 250 m window is used, and data are padded to 10,000 data points. 3–2 MTM (Multitaper-Method spectral analysis) spectra were calculated (Meyers, 2014; Rahim et al., 2014; Thomson, 1982) of interpolated and detrended time series. MTM spectral analysis is an often used method to detect cyclic components in (geologic) data; it represents the transformation from a time series to a power spectrum where the cyclic components are represented by enhanced spectral power.

ASM (Average Spectral Misfit; Meyers and Sageman, 2007; Meyers et al., 2012) was applied to find if there is a theoretically optimal average sedimentation rate that would match the observed cycles (in meters) to Milankovitch periodicities.

Sedimentation rates between 50 and 120 cm/kyr were tested. The target was constructed from an ETP (mix with equal contributions from eccentricity, tilt and precession) from the 13.8–14.8 Ma interval with all frequencies <0.01 [1/kyr]. All frequencies of <0.1 significance and $>90\%$ confidence using a harmonic F-test from data are used in the ASM. The ASM assumes constant sedimentation rate over a tested depth interval, which may not be strictly the

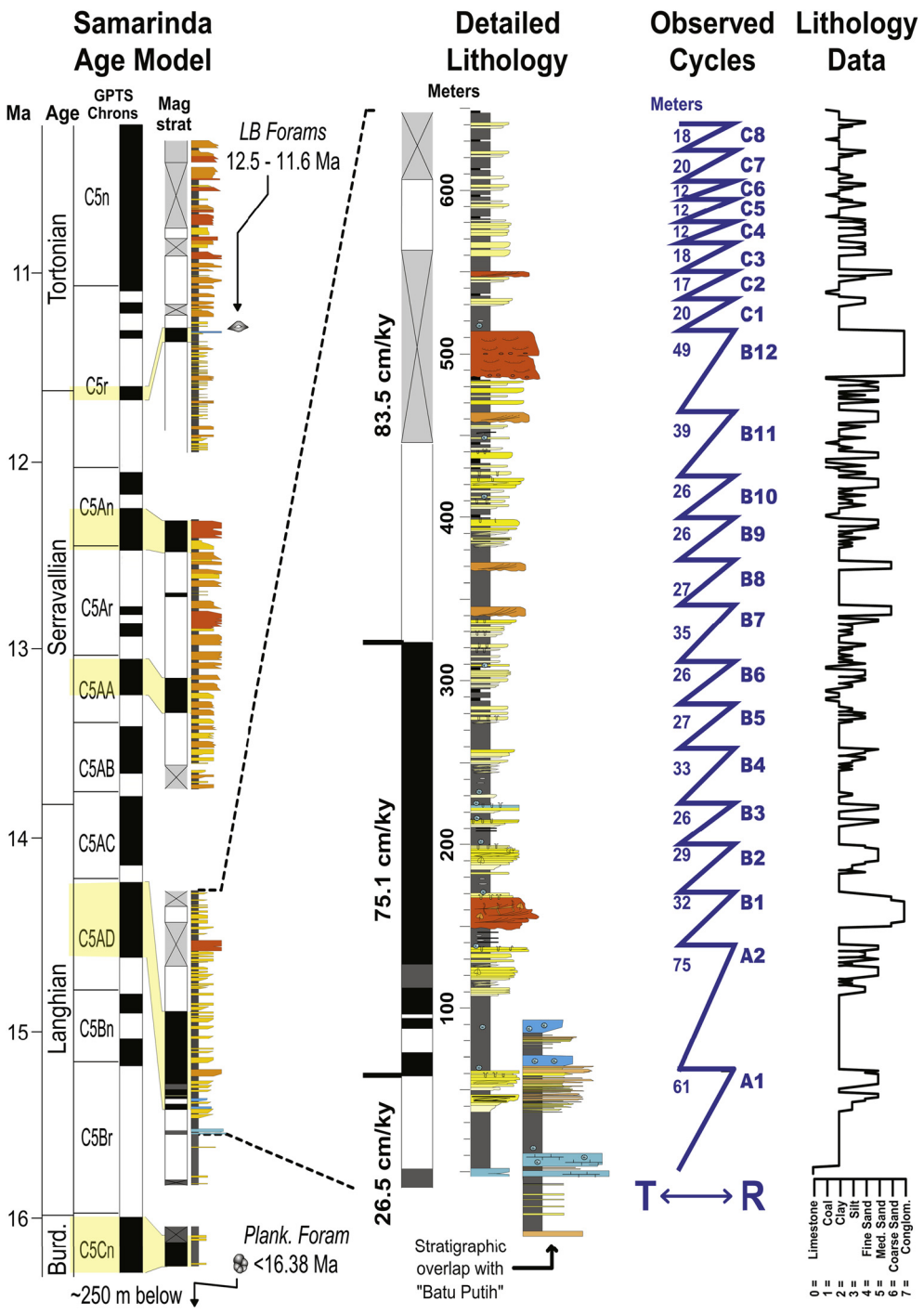

Fig. 4. The age model of Marshall et al. (2015) is summarized (left). The detailed stratigraphic log of Sungai Kunjang with magnetostratigraphy and the calculated sedimentation rates (center). See Supp. Fig. 1 for a much more detailed drawing of the log. The interpreted Transgressive–Regressive cycles are shown and with meters on the left and names on the right. The lithology data used for statistical analysis is shown (right).

case especially in deltaic systems where intervals of coarser material input may result in higher sedimentation rates than aggradation phases. However, the mean sedimentation rate over a cycle may remain constant.

4. Results

4.1. Observed cycles

The cycles show different thicknesses and may be divided into three groups (Fig. 4). 'A cycles' occur in the lower 150 m of the section (including the correlated lower portion of the Batu Putih section) and are relatively thick: 61, and 75 m. The A cycles terminate with thick sandstone. 'B cycles' occur between 150 m and 500 m stratigraphically and are regularly spaced; not deviating far from a 30 m thickness. B11 and B12 are notably thicker (~40 and 50 m), generally more sandy, and culminate in the thickest and coarsest sandstone in the section. 'C cycles' follow above 500 m and have less coarse and thinner sandstone, and are more tightly spaced (12–20 m). Coal intervals become increasingly common within cycles above 400 m stratigraphically.

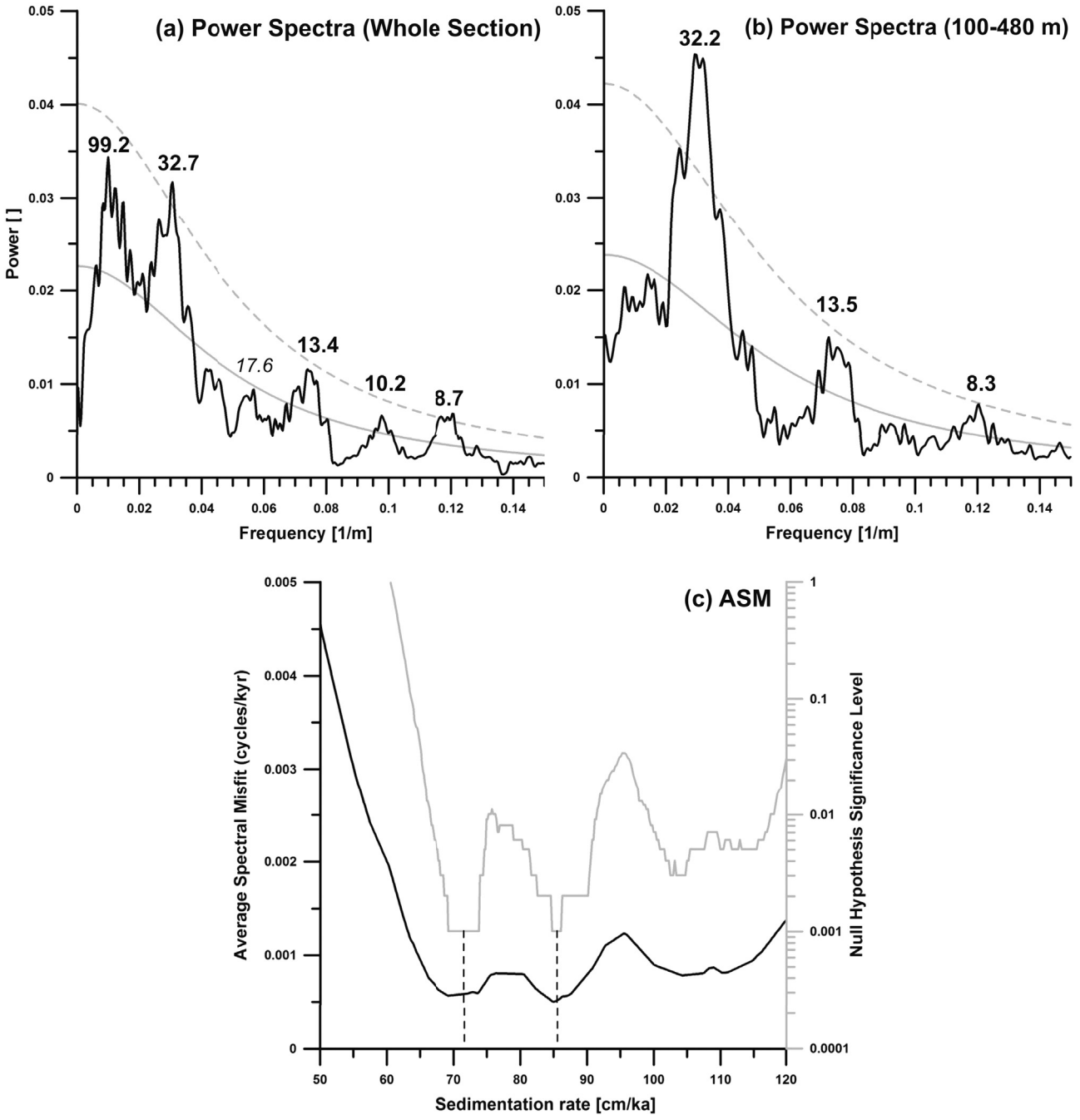

Fig. 5. MTM spectra of interpolated depth series for the whole section (left), and the 100–480 m interval associated with the "B cycles" (middle). In both cases, thin solid dashed lines indicate the 90% and 95% confidence thresholds, respectively. In the right panel ASM (black line) and null hypothesis (grey line) was applied to the depth series; sedimentation rates of ~72 and ~85 cm/kyr give highly significant matches with orbital targets, highlighted with dashed lines.

4.2. Outcome of statistical analysis in the stratigraphic domain

4.2.1. Power spectra

Power spectra (3–2 MTM spectra; Meyers, 2014; Rahim et al., 2014; Thomson, 1982) were generated for the whole stratigraphic interval and for the subdivisions corresponding to the B cycles (Fig. 5a, b). In the power spectrum of the whole section, elevated power occurs at around 70–100 m cycle (peaking around 99 m), probably corresponding to the A cycles. A strong spectral peak is found at ~30 m, corresponding to the B cycles. Further intervals of increased power occurs around 13, 10, and 8 m. A very weak peak is further present at ~18 m, which doesn't exceed the 90% confidence window. The power spectrum of the 100–480 m interval shows that a strong 30 m B cycle peak exceeding the 95% confidence level. Additionally, ~13 m and ~8 m cycles are detected by this analysis that were not initially recognized, but suggest that the alternations in minor silt/sandstone beds with shale are not random.

4.2.2. Wavelet analysis

The resulting wavelet contour graph from the lithology data reveals distinct cyclicity (red to brown colored) in the approximate period bands of 16, 30 and 90 m (Fig. 6). Wavelet analysis indicates the presence of ~30 m cyclicity occurring between 100 and 400 m stratigraphically, further confirming the 30 m B cycles. Even though there is a decrease in power at this frequency between 230 m and 320 m, an interval associated with overall finer sandstones. Above 400 m, power shifts to a higher frequency of

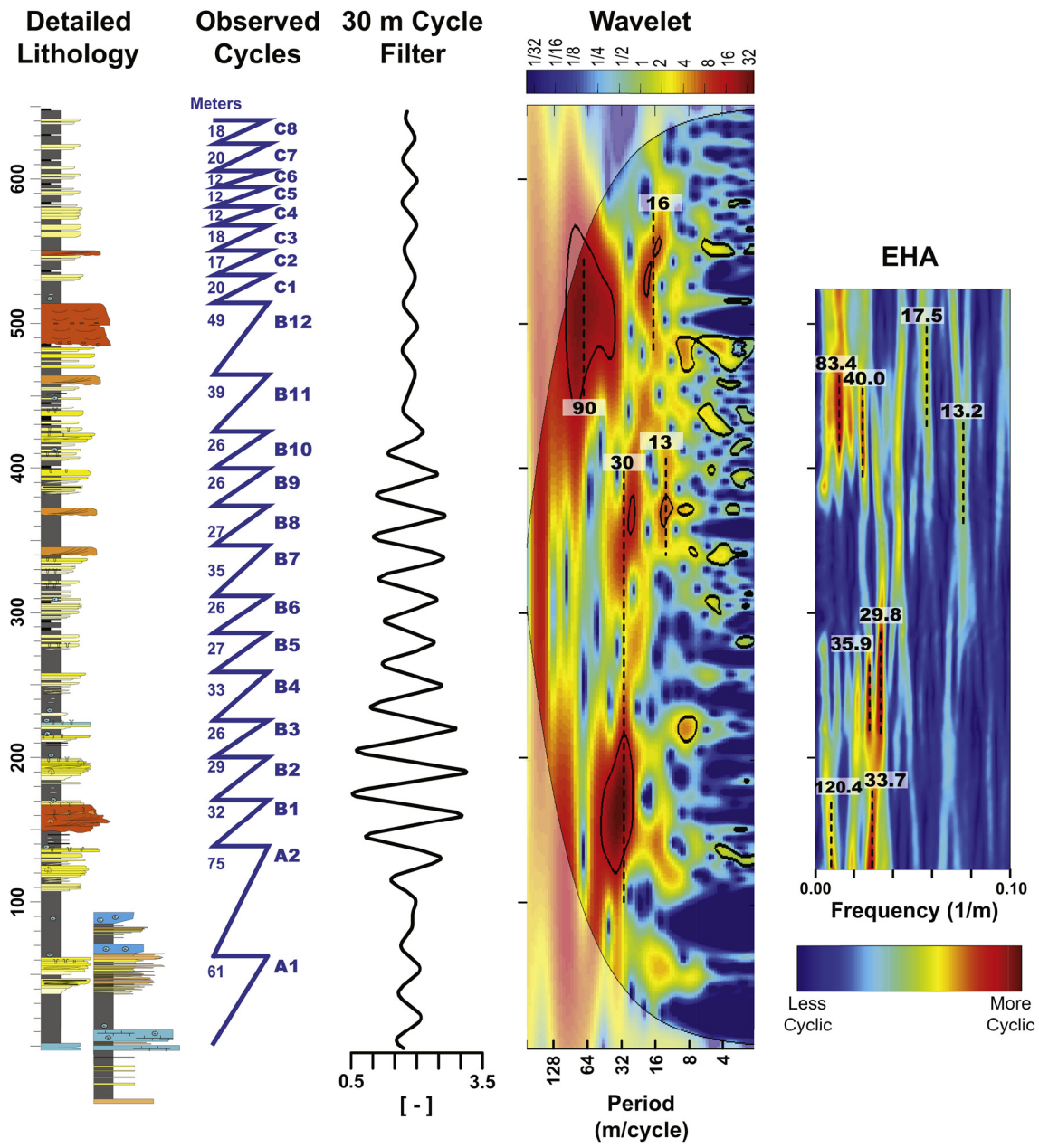

Fig. 6. Lithologic log and observed cycles (left) compared to the resulting 30 m Cycle Filter, Wavelet analysis, and Evolutive harmonic analysis (EHA): Filtering for ostensible 30 m cyclicity utilizes taner bandpass filters from 0.0286 [1/m] to 0.04 [1/m] and 0.0125 [1/m] to 0.01 [1/m] and roll-off rates of 105. Wavelet analysis plotted with red and brown coloration indicating a strong occurrence of a periodicity. EHA of the 'depth' series with strong periodicities indicated. Due to the 250 m window, no EHA is available for the lower- and uppermost parts of the section. Dashed lines with their respective periodicity in meters highlights the strong periodicities found by Wavelet and EHA. (For interpretation of the references to color in this figure legend, the reader is referred to the web version of this article.)

around 16 m, which corresponds to the C type cycles with an average thickness of 16.1 m, and also to the minor sandstone-shale alternations, between 400 and 500 m, although not as strongly. A brief but noticeable increase in power of a 13 m cycle also occurs around 470 m, which is probably reflecting minor sandstone-shale alterations and perhaps is related to the subsequent 16 m cycle band. Additionally present is a strong increase in power around a period of ~90 m, above 400 m. The filter of the ~30 m component shows highest amplitudes from ~100 to 450 m, highlighting the B cycles, and is weak during the intervals of A and C cycles (Fig. 6).

4.2.3. Evolutive harmonic analysis

EHA supports the findings from wavelet analysis, also finding ~30 m cyclicity between 100 and 300 m corresponding to the observed B cycles, ~17 m cycles above 400 m corresponding to the observed C cycles and an intriguing increase in power at the ~80–90 m period above 400 m (Fig. 6). Additionally, EHA shows weaker increases in power at ~13 m above 300 m which correlates to the presence of high frequency alternations of fine sand and silt with shale in that interval. The power increase for a 40 m periodicity above 400 m might be a statistical frequency modification of the 30 m B cycles caused by the abnormally thick cycles B11 and B12 (Fig. 6). A 120 m cycle is recorded below 200 m.

4.2.4. Average spectral misfit

The average spectral misfit (ASM; Meyers and Sageman, 2007; Meyers et al., 2012) seeks for the best and most significant correspondence of observed peaks in power spectra with Milankovitch frequencies through an ensemble of sedimentation rates. Sedimen-

Table 1
Calculated time-periodicties for the statistically determined cycles, using the two sedimentation rates determined by ASM (Fig. 6c). For comparison, the typical periodicities of precession, obliquity and eccentricity cycles is shown on the right-most side.

Cycle periodicity (m)	Sedimentation rate (cm/kyr)		Milankovitch cycles
	72	85	
13	18.1 kyr	15.3 kyr	Precession
16	22.2 kyr	18.8 kyr	23–25 kyr
30	41.7 kyr	35.3 kyr	Obliquity 41 kyr
68	94.5 kyr	80.0 kyr	Eccentricity
90	125.0 kyr	105.9 kyr	95–125 kyr

tation rates ranging from 50 to 120 cm/kyr (Fig. 5c) were tested. There are two distinct optimal fits for the Sungai Kunjang section with average sedimentation rates of ~72 and ~85 cm/kyr (Fig. 5c).

5. Discussion

5.1. Cyclostratigraphy

Marshall et al. (2015) estimated the sedimentation rate of the Batu Putih limestone at the base of the section to be between 20 and 40 cm/kyr. This range in sedimentation rates results from uncertainties in the position of the inferred Chron C5Bn boundaries in the integrated stratigraphy of the area (Marshall et al., 2015). Above this, the estimated sedimentation rate increases from ~75 cm/kyr in the lower half to ~85 cm/kyr upper half ("model A" in Marshall et al., 2015). Sedimentation rates from onshore wells in the region give similar estimates of 60 to 100 cm/kyr after 15.5 Ma (Witts et al., 2015). The two sedimentation rates calculated by ASM (~72 and ~85 cm/kyr) are a close match to these estimates. The appearance of two ASM significance maxima at ~72 and 85 cm/kyr sedimentation rate might be indicative of the sedimentation rate change proposed my Marshall et al. (2015), although it does not support a lower sedimentation rate of <50 cm/kyr in the lowest part of the section around the Batu Putih limestone. It is important to note that ASM here represents the average sedimentation rate, and that sedimentation rates may be different especially in the stratigraphic intervals of 1–100 m, and 480–650 m. Sedimentation rates can also be expected to have varied with lithology, and may have been higher in the coarser lithologies as observed in similar settings (e.g. Valero et al., 2015). Sedimentation rate can be assumed to be similar between cycles, even though it is likely highly variable within cycles. As such, ASM is sensitive to the relative duration of cycles and cyclic sedimentation can be expected not to change the ratios between the thicknesses of precession, obliquity and eccentricity related sedimentary cycles as compared to the timing ratio of the astronomical movements significantly.

The stratigraphic cycles highlighted by statistical analysis are converted to time periods using both the sedimentation rates calculated by ASM analysis (72 and 85 cm/kyr) shown in Table 1. In both cases the periods match those of Milankovitch time bands; a particularly good match is obtained for 72 cm/kyr. The 13 and 16 m cycles associated with the C cycles and high frequency minor sandstone alternations found elsewhere are roughly 20 kyr in duration and likely correspond to precession. The prominent 30 m B cycles convert to a ~42 kyr period that is congruent with obliquity. The two A cycles have an average thickness of 68 m, with a calculated period of 80–95 kyr, matching the ~95 kyr eccentricity. If the sedimentation rate changes from 75 to 85 cm/kyr in the middle of the section as suggested by Marshall et al. (2015), the cycle durations fit those of the Milankovitch cycles better. For instance, a sedimentation rate of 72 cm/kyr produces a periodicity of around 95 kyr for the A cycles, as opposed to 80 kyr if the sedimentation rate was higher at 85 cm/kyr. The presence of both 13 and 16 m cycles might also be a reflection of a sedimentation rate change. Both wavelet analysis and EHA show that 13 m cycles occur around 350 to 500 m, with 16–17 m cycles appearing generally above.

Hence, the time periodicities resulting from the estimated sedimentation rates fall within the Milankovitch frequency bands and show a progression from eccentricity (A cycles) to obliquity (B cycles) and finally precession (C cycles) dominance. It also appears that the initially unnamed smaller alternations in minor sandstone beds below 500 m are also precession driven, indicating that there is an interval between 300 m and 500 m in which both precession and obliquity cycles are present.

5.2. Comparison to global climate records

Astronomical calculations and also open-ocean climate proxy records provide an opportunity to see what kind of cyclicity may be expected, in the time interval between 15.5 and 13.5 Ma. Benthic isotope data from Integrated Ocean Drilling Project (IODP) sites (i.e. Pacific and China Sea Sites 1146, 1147, 1236, 1237, 1338) provide high resolution records of the middle Miocene climate imprint of astronomical forcing (Holbourn et al., 2007, 2013, 2014). These records indicate that ~100 kyr eccentricity and precession related cycles dominate before ~14.7 Ma and after ~13.8 Ma, while the 40 kyr obliquity cycle is dominant between 14.7 and 13.8 Ma (Fig. 7). Gamma ray log data from the middle Miocene Pearl River Mount Basin and its distal delta system, in the South China Sea, also shows a similar progression from eccentricity, to obliquity, and finally precession, during the same time period, including a dramatic shift around 13.8 Ma (Fig. 8; Tian et al., 2013). Furthermore, gamma ray log and magnetic susceptibility data from the Ceara Rise (ODP Sites 925–926) reveals a similar shift from obliquity to precession/eccentricity influence after 13.8 Ma as well (see Supp. Mat.; Shackleton et al., 1999; Zeeden et al., 2013). The same shifts are also found in sedimentary cycle patterns in the Mediterranean (see Supp. Mat.; Hüsing et al., 2010) and may thus be regarded as global. The relatively strong obliquity in between is due to a long term 2.4 Myr eccentricity minimum centered around 14.3–14.4 Ma combined with a long term 1.2 Myr obliquity maximum around the same time (see also Holbourn et al., 2007, their Fig. 5).

In the Sungai Kunjang record, the apparent change from thicker and longer A cycles to the thinner and shorter cycles is interpreted to reflect a change from eccentricity to obliquity at around 150 m. Based on the age model of Marshall et al. (2015), this change occurs just before 14.5 Ma, which is in excellent agreement with the Pacific, Atlantic and Mediterranean records and the astronomical forcing, all showing the same frequency change at 14.7 Ma. In the (I)ODP records and also Chinese loess (Hao and Guo, 2007), a change in dominant cyclicity from obliquity to precession occurs at around 13.8 Ma. In the Sungai Kunjang record, a shift towards higher frequencies is observed above 500 m, with an age of 13.7–14 Ma. Thus, global climate records are showing the same changes in cycle duration as seen in the Sungai Kunjang record, giving further support that deltaic sedimentation was strongly influenced by global climate cycles caused by orbital forcing.

Given the good match in the changes of the dominant cyclicity, the next step is to investigate if a direct and unambiguous correlation between Sungai Kunjang and the global signal can be made. The ~14.7 Ma change from eccentricity to obliquity in the benthic $\delta^{18}O$ record of IODP Site 1338 (Holbourn et al., 2014) can be correlated to the eccentricity/obliquity transition seen at Sungai Kunjang which has a similar age estimate of 15 Ma or is slightly younger (Marshall et al., 2015). In addition, the transition from

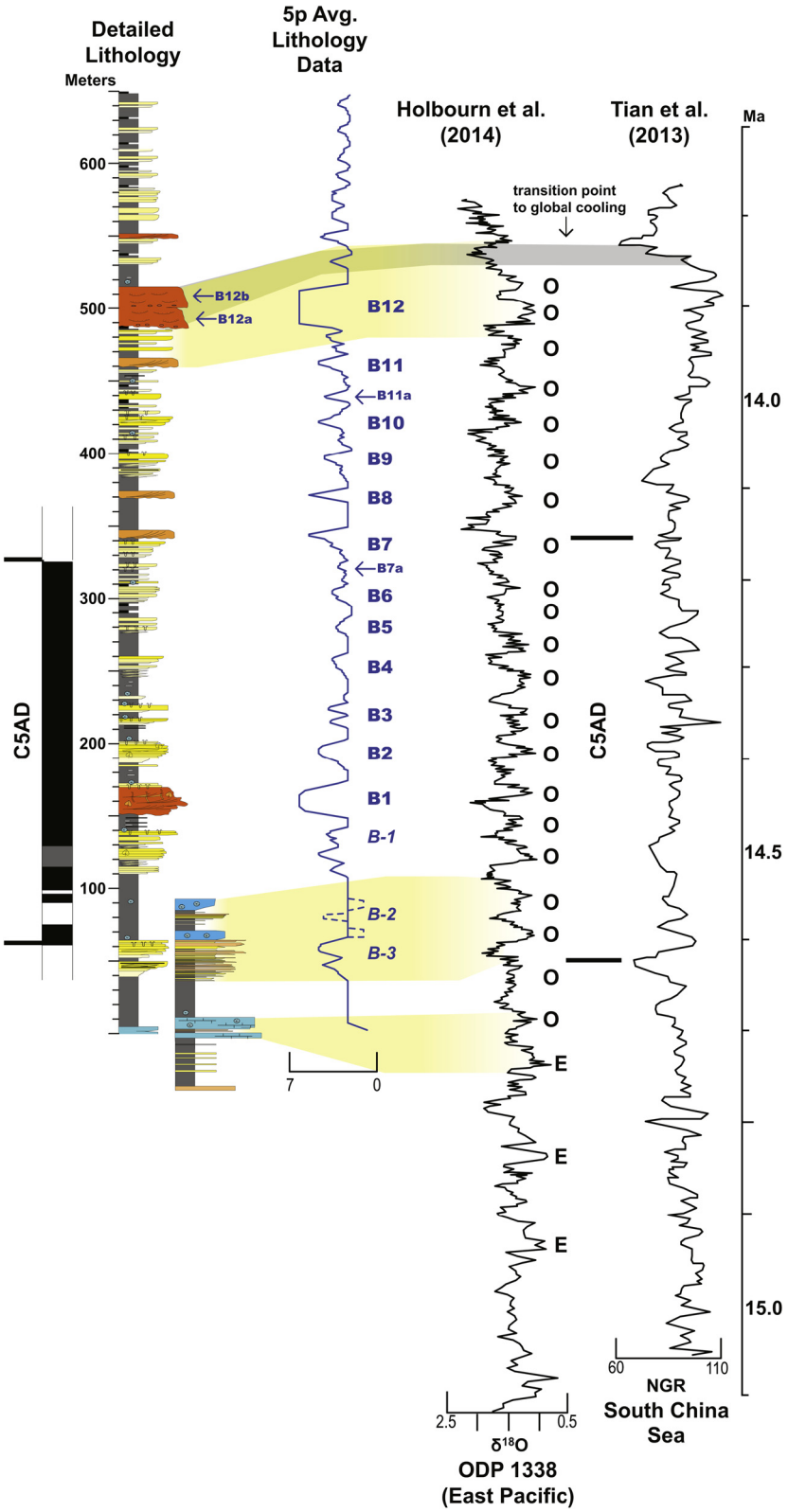

Fig. 7. Lithologic log and the 5-point moving average of the lithology data (left) compared to climate records (right). Dashed lines in the lithology data indicates possible 'B' cycles better developed in the Batu Putih section, overlooked in the analysis of the Sungai Kunjang section. (I)ODP site 1338 shows very clear Milankovitch cycles; the most pertinent Eccentricity (E) and Obliquity (O) cycles are noted, as are yellow highlights showing the suggested tie-points to the Sungai Kunjang section and a grey highlight showing the location of the key sea-level drop event at ~13.8 Ma. Also shown is gamma ray (NGR) data from an offshore delta in the northern South China Sea. Supplemental Fig. 2 provides more climate records, from other locations, for comparison. The C5ADn chron on all records is shown to illustrate the very similar dominance of obliquity to the lower B cycles, including additional ones better seen at the Batu Putih location, and potentially missed cycles in B7, B11 and B12. (For interpretation of the references to color in this figure legend, the reader is referred to the web version of this article.)

obliquity to precession can be used as tie point. The best match between the Sungai Kunjang section and IODP Site 1338 is shown in Fig. 7. The IODP record contains 20 obliquity cycles in between these points, while the Sungai Kunjang section only contains 12 B cycles in the same interval, indicating that nine obliquity cycles are missing. The Batu Putih section more clearly portrays environmental changes in the equivalent portion of the Sungai Kunjang record (between 50 and 100 m) which adds potentially two obliquity cycles (B-1, B-2 in Fig. 7). It is further possible, that some obliquity related cycles in our record are obscured by noise or a less distinct expression of the cyclicity. The thicker than average cycles B7 and B11 provides examples of this as they have several minor beds within the "shale" interval, which potentially represents two obliquity cycles that were not initially recognized (note B7a and B11a in Fig. 7). This might account for two more obliquity cycles. Finally, the B cycles interval ends with a very thick cycles (B12) and very thick conglomeratic sandstone bed (at ∼500 m) that shows evidence of sedimentary cannibalism such as inter-sandstone-channeling and reworked sandstone clasts (Cibaj, 2009). It is also the thickest sandstone, further supporting a partly different origin than the thinner sandstone beds below. The characteristics may be indicative for the presence of a hiatus in the section, which would account for some of the missing cycles. The bed shows a noticeable parting about half way, which may account for at least two cycles amalgamated into a single bed (noted at B12a, b in Fig. 7). Conceivably, the loss of cycles may even be expected given the marked shift to heavier benthic δ^{18}O values at around 13.8 Ma and the associated substantial (40–70 m) sea level drop (John et al., 2011; De Boer et al., 2012; Levy et al., 2016). Such a major lowering of sea level would allow fluvial sediments to prograde under erosive conditions, potentially resulting in the amalgamation or removal of cycles. However, the minimum number of three missing cycles corresponds to a thickness of approximately 90 m that is too high to be solely explained by erosion caused by the global sea-level drop. Consequently, other mechanisms such as autogenic river avulsion of delta lobe migration and/or regional tectonism have to be involved to explain the full loss of sedimentary cycles. The rather well defined magnetostratigraphic interval that corresponds to C5ADn contains several 30 m cycles (Fig. 7). Including extra cycles better seen in the Batu Putih section (B-1, B-2 and B-3), the 446 kyr interval of C5AD contains 10 cycles at 44.6 kyr per cycle. However, same interval in ODP Site 1338 record contains 12 obliquity cycles (Fig. 7). Some cycles may be missing because of the change to a more proximal setting from the reef/slope environment which was potentially controlled by another order of cyclicity or tectonics.

The lack of complete obliquity related cycles is not an issue for spectral analysis and the identification of periodicity. However, the presence of incomplete cycles might be a source of error in spectral analysis, as these cycles will likely span less thickness than fully recorded cycles. Nevertheless, the Sungai Kunjang section contains enough full cycles to calculate their approximate periodicity and attempt to correlate them to records of global climate change, even though unequivocal correlations remains out of reach.

5.3. Allogenic Milankovitch forcing

The Kutai Basin was tectonically active during the Miocene, undergoing basin inversion, while uplift in the interior of Borneo occurred throughout the middle Miocene. On a larger time scale (i.e. 15 Ma to present), well data indicate major shelf break migration events with a 2–5 Myr recurrence that do not necessarily match major global climate events and show a departure from the aggradational stacking of finer scale basin sedimentation (Cibaj et al., 2014). Cibaj et al. (2014) proposes that these shelf break migration events are driven by pulses of tectonic compression. However, tectonic changes typically take place at rates that are an order of magnitude slower than the Milankovitch periodicities examined here, and would not explain the match to global climate records (Miller et al., 2005).

Time series analysis strongly suggests that orbital climate forcing exerted major control on the paleo-Mahakam Delta; the further question is whether upstream (rainfall) or downstream (eustatic) mechanisms are dominant. Studies from the Pleistocene of the Mahakam Delta point to glacioeustatic control by the ∼100 kyr eccentricity cycle as carbonate buildups match with climate records of glacial terminations and sea level rise, which held back sediment and/or reduced sediment load under drier climate of glacial terminations, allowing reefs to form (Saller et al., 2004). During sea level rise, marine muds were deposited across the shelf with carbonates forming on the shelf edge. Upon stabilization during highstand and eventual fall of sea levels, the delta prograded across the shelf, with subsidence aiding to produce accommodation space for this depositional regime. On reaching the shelf edge, the prograded sediments stacked onto the upper slope as a lowstand delta, with no definable sequence boundary between the highstand and lowstand. This description of the Pleistocene sequences can be used for the cyclic aggrading sediment packages of similar depositional facies (deltaic cycles) studied here, although in a more proximal setting. The Batu Putih reef shows evidence of drowning, as do other Miocene reefs in the region (Marshall et al., 2015; Santodomingo et al., 2015).

As seen in the Pleistocene, reef formation in the Miocene occurred during transgression, but was successively drowned as relative sea levels rose further. During highstand and regression, the delta prograded. Poorly defined boundaries between highstand and lowstand are seen in the Miocene succession. In the upper half of the section, carbonate and marine fauna is often missing, and highstand shale rests below lowstand deposits that also start with shale, making this transition obscured. This boundary is sometimes still visible as a thin coaly layer. The similarity in the progression of the sedimentation style in the Pleistocene (100 kyr) and Miocene cycles, gives some support that they were controlled by similar mechanisms, pointing to sea level control. Another interesting factor is the erosive and coarse nature of the sandstone beds, pointing to abrupt changes in sediment supply and periods of exposure (Cibaj, 2009). This might be explained by sea level fall, prompting a drop in base-level and triggering erosion. A dominant control by sea level may also explain the strong obliquity signal which is atypical for the tropics from a conceptual point of view, because tropical (summer) insolation is thought to be dominated by precession (but see below).

The last several 100 kyr sea-level changes are estimated to be up to or exceeding of 100 m, which is a palpable mechanism for driving major sedimentary change (De Boer et al., 2012). Estimates of sea-level fluctuations during the middle Miocene, besides the major drop at ∼13.8 Ma, are less than in the Pleistocene, <40 m (Miller et al., 2005; De Boer et al., 2012; Gasson et al., 2016). However, modeling studies show that global gravitational distribution of water from melting terrestrial ice might affect the Indo-pacific region more than other locations, thus sea level changes can be expected to have been greater than the average (e.g. Spada et al., 2013).

An alternative to glacioeustatic control is variations in monsoonal precipitation governing fluvial activity. The interval of obliquity dominance at Sungai Kunjang (roughly 14.6–14.0) occurs during a period of obliquity control seen in multiple IODP climate proxy records that point to glacioeustatic sea level change (Holbourn et al., 2007, 2013, 2014). Climate modeling of orbital extremes indicates that both precession and obliquity have a marked effect on low-latitude monsoonal systems, whereby the obliquity signal is explained by cross-equatorial moisture transport, adding

winter insolation in the opposite hemisphere to the mechanism of monsoonal intensification (Bosmans et al., 2015). Such obliquity dominance can also be observed in low-latitude records of younger Miocene age, although these are not necessarily controlled by low-latitude processes (e.g. Zeeden et al., 2013). Importantly, a recent IODP study in the South China Sea from 15.5 to 13 Ma (Holbourn et al., 2015), demonstrates that the orbital forcing seen in the surface water oxygen isotope record was driven in particular by wet/dry climate fluctuations; these occur not in sync with benthic oxygen isotope cyclicity which is tied to polar ice sheet growth (Holbourn et al., 2015). Thus, sandy delta lobe progradation plausibly occurred during intense monsoon periods with low energy clayey delta plain and peat swamps dominating during weaker monsoon periods.

A high resolution palynology study found that the Kutai Basin region experienced a perennially wet climate throughout the late Miocene, showing minimal evidence for vegetation changes that would indicate wet/dry fluctuations (Morley and Morley, 2011). This study suggested that pollen changes reflected coastal vegetation responding to 100 kyr sea level change. As the Early and Middle Miocene were generally warmer and wetter periods globally, it is probable that the Kutai Basin area was also ever-wet in the Middle Miocene (Morley and Morley, 2011). Thus, the pollen record from the Kutai Basin suggests that in the Miocene wet-dry fluctuations in the region were not a strong influence compared to coastal migration caused by sea-level change. Alternatively, it would be between wet and very wet, if upstream rainfall oscillations were the controlling factor.

6. Conclusions

Statistical analysis confirms the existence of decameter cycles in the shallow marine to deltaic Sungai Kujang record from the middle Miocene of Borneo. This includes ~30 m cycles throughout the middle part of the section as well as 13–17 m cycles in the upper 250 m of the section. When these cycle thicknesses are converted to time using independently determined sedimentation rates of 75–85 cm/kyr confirmed independently by ASM, these cycles reflect ~40 kyr and 20 kyr cycles, respectively, which are consistent with obliquity and precession forcing. We suggest that the lower portion of the section has lower sedimentation rates, and the ~68 m cycles are related to 100 kyr eccentricity. Marine records of climate change reveal a progression from eccentricity to obliquity to procession/eccentricity occurs during the time interval between 15 and 14 Ma, giving credence to the eccentricity–obliquity-precession pattern seen in the Sungai Kujang section.

It appears that the thick, conglomeratic sandstone at 500 m might record the timing of a substantial global sea level drop associated with a major climatic cooling event and expansion of the EAIS. It is suggested that this dramatic increase in coarse sediment deposition represents increased erosion and proximal deposition, driven by enhanced runoff and sea level fall. This exceptional bed likely represents a hiatus, which in turn may explain some of the missing obliquity controlled cycles in the Sungai Kujang section compared to climate proxy records from the open ocean. Nevertheless, the presence of the same cyclic progression in the deltaic setting presented here, highlights the importance of orbital forcing during this time period of warmer yet rapidly changing (i.e. cooling) climate and across a spectrum of latitude and sedimentary environments.

Given the similarities in the cycle architecture between in the Miocene Sungai Kunjang cycles and Pleistocene cycles in the Kutai Basin that are tied to glacioeustatic changes, it seems likely that glacioeustatic oscillations played a prominent role in controlling sedimentation in this Miocene equatorial delta, even at the time of a warmer climate and a different global ice sheet configuration. However, astronomically induced climate driven changes in precipitation, discharge and sediment transport cannot be discounted.

Furthermore, our study suggests that the (Batu Putih) patch-reef harboring the emerging biodiversity hotspot in SE Asia is possibly associated with eccentricity driven minima in terrigenous sedimentation around 14.7 Ma, tying glacioeustatic sea level rise that held back turbidity, as a key factor in reef formation in this dynamic region of the Indonesia Archipelago. Our findings must also be considered in the context of the long term tectonic control on the basin, which provided accommodation space and the steadily high sediment rates that allowed for the recording of the high frequency Milankovitch cycles and potentially accounted for lower order (millions of years) cycles of sedimentation.

While study of more proximal settings would shed light on the potential contribution of such regional climate oscillations and/or the upstream response to potential base level changes, it will be difficult to assess these relationships as the proximal facies are not preserved because of erosion and/or not well exposed. An important logical next step is to include subsurface and offshore records for comparison with the records presented here to see how sediments and microfauna might have varied cyclically, potentially giving further clues to the complex mechanisms at play.

Acknowledgements

We would like to thank the Marie Curie Actions Plan, Seven Framework Programme (Grant no. 237922) for the funding that made this project possible; and the Indonesian geological survey for their assistance with logistics and fieldwork. A special thanks to the late Irfan Cibaj for his vital guidance in the field and sedimentological discussion.

Appendix A. Supplementary material

Supplementary material related to this article can be found online at http://dx.doi.org/10.1016/j.epsl.2017.04.015.

References

Abels, H.A., Kraus, M., Gingerich, P.D., 2013. Orbital climate cycles triggering river avulsion in the lower Eocene Willwood formation, Bighorn Basin, Wyoming (USA). Sedimentology 60, 1467–1483.

Badger, M., Lear, C., Pancost, R., Foster, G., Bailey, T., Leng, M., Abels, H., 2013. CO_2 drawdown following the middle Miocene expansion of the Antarctic Ice Sheet. Paleoceanography 28, 42–53.

Bosmans, J., Drijfhout, S., Tuenter, E., Hilgen, F., Lourens, L., Rohling, E., 2015. Precession and obliquity forcing of the freshwater budget over the Mediterranean. Quat. Sci. Rev. 123, 16–30.

Bowman, A., Johnson, H., 2014. Storm-dominated shelf-edge delta successions in a high accommodation setting: the palaeo-Orinoco Delta (Mayaro Formation), Columbus Basin, South-East Trinidad. Sedimentology 61, 792–835.

Cibaj, I., 2009. A fluvial series in the middle Miocene of Kutei Basin: a major shift from proto-Mahakam shallow marine to the continental environment: AAPG Hedberg Conference publication, April 29. http://www.searchanddiscovery.com/pdfz/abstracts/pdf/2010/hedberg_indonesia/abstracts/ndx_cibaj.pdf.html.

Cibaj, I., 2013. Miocene stratigraphy and paleogeography of lower Kutei Basin, East Kalimantan – A Synthesis. In: Proceedings From the Indonesian Petroleum Association Convention. http://archives.datapages.com/data/ipa_pdf/084/084001/pdfs/IPA13-G-090.htm, 2013.

Cibaj, I., Lambert, B., Zaugg, P., Ashari, U., Dal, J., Imbert, P., 2014. Stratigraphic stacking patterns of the Mahakam Area, lower Kutei Basin, East Kalimantan, Indonesia. In: Proceedings From the Indonesian Petroleum Association Convention. http://archives.datapages.com/data/ipa_pdf/2014/IPA14-G-145.htm.

Chambers, J., Daley, T., 1997. A tectonic model for the onshore Kutai Basin, East Kalimantan. In: Fraser, A.J., Matthews, S.J., Murphy, R.W. (Eds.), Petroleum Geology of Southeast Asia. Geol. Soc. (Lond.) Spec. Publ. 126, 375–393.

Coe, Angela L., Bosence, Dan W.J., Church, Kevin D., Flint, Stephen S., Howell, John A., Wilson, Chris L., 2003. The Sedimentary Record of Sea-Level Change, 1st ed. Cambridge University Press.

De Boer, B., Van De Wal, R., Lourens, L., Bintanja, R., 2012. Transient nature of the Earth's climate and the implications for the interpretation of benthic $d^{18}O$ records. Palaeogeogr. Palaeoclimatol. Palaeoecol. 335–336, 4–11.

Diessel, C., 2006. Utility of coal petrology for sequence-stratigraphic analysis. Int. J. Coal Geol. 70, 3–34.
Flower, B., Kennett, J., 1994. The middle Miocene climatic transition: East Antarctic ice sheet development, deep ocean circulation and global carbon cycling. Palaeogeogr. Palaeoclimatol. Palaeoecol. 108, 537–555.
Gasson, E., DeConto, R.M., Pollard, D., Levy, R.H., 2016. Dynamic Antarctic ice sheet during the early to mid-Miocene. Proc. Natl. Acad. Sci. USA 113, 3459–3464.
Grinsted, A., Moore, J.C., Jevrejeva, S., 2004. Application of the cross wavelet transform and wavelet coherence to geophysical time series. Nonlinear Process. Geophys. 11, 561–566.
Hall, R., 2009. The Eurasian SE Asian margin as a modern example of an accretionary orogen. Geol. Soc. (Lond.) Spec. Publ. 318, 351–372.
Hall, R., 2012. Late Jurassic-Cenozoic reconstructions of the Indonesian region and the Indian Ocean. Tectonophysics 570–571, 1–41.
Hall, R., Nichols, G., 2002. Cenozoic sedimentation and tectonics in Borneo: climatic Influences on Orogenesis. In: Jones, S.J., Frostick, L. (Eds.), Sediment Flux to Basins: Causes, Controls and Consequences. Geol. Soc. (Lond.) Spec. Publ. 191, 5–22.
Hao, Q., Guo, Z., 2007. Magnetostratigraphy of an early-middle Miocene loess-soil sequence in the western Loess Plateau of China. Geophys. Res. Lett. 34.
Hilgen, F.J., Hinnov, L.A., Abdul Aziz, H., Abels, H.A., Batenburg, S., Bosmans, J.H.C., De Boer, B., Hüsing, S.K., Kuiper, K.F., Lourens, L.J., Rivera, T., Tuenter, E., Van de Wal, R., Wotzlaw, J-F., Zeeden, C., 2014. Stratigraphic continuity and fragmentary sedimentation: the success of cyclostratigraphy as part of integrated stratigraphy. Geol. Soc. (Lond.) Spec. Publ. http://dx.doi.org/10.1144/SP404.12.
Holbourn, A., Kuhnt, W., Schulz, M., Flores, J., Andersen, N., 2007. Orbitally-paced climate evolution during the middle Miocene "Monterey" carbon-isotope excursion. Earth Planet. Sci. Lett. 261, 534–550.
Holbourn, A., Kuhnt, W., Frank, M., Martin, J., Haley, B., 2013. Changes in Pacific Ocean circulation following the Miocene onset of permanent Antarctic ice cover. Earth Planet. Sci. Lett. 365, 38–50.
Holbourn, A., Kuhnt, Wolfgang, Lyle, Mitch, Schneider, Leah, Romero, Oscar, Andersen, Nils, 2014. Middle Miocene climate cooling linked to intensification of eastern equatorial Pacific upwelling. Geology 42, 19–22.
Holbourn, A., Kuhnt, W., Regenberg, M., Schulz, M., Mix, A., Andersen, N., 2015. Does Antarctic glaciation force migration of the tropical rain belt? Geology 38, 783–786.
Hüsing, S.K., Hilgen, F.J., Kuiper, K.F., Krijgsman, W., Turco, E., Cascella, A., Wilson, D., 2010. Astrochronology of the Mediterranean Langhian between 15.29 and 14.17 Ma. Earth Planet. Sci. Lett. 290, 254–269.
John, C.M., Karner, G., Browning, E., Leckie, M., Mateo, Z., Carson, B., Lowery, C., 2011. Timing and magnitude of Miocene eustasy derived from the mixed siliciclastic-carbonate stratigraphic record of the northeastern Australian margin. Earth Planet. Sci. Lett. 304, 455–467.
Kodama, K.P., Anastasio, D.J., Pares, J., Hinnov, L.A., 2010. High-resolution rock magnetic cyclostratigraphy in an Eocene flysch, Spanish Pyrenees. Geochem. Geophys. Geosyst. 11, 1–22.
Levy, R., Harwood, D., Florindo, F., Sangiorgi, F., Tripati, R., Von Eynatten, H., Gasson, E., Kuhn, G., Tripati, A., DeConto, R., Fielding, C., Field, B., Golledge, N., McKay, R., Naish, T., Olney, M., Pollard, D., Schouten, S., Talarico, F., Warny, S., Willmott, V., Acton, G., Panter, K., Paulsen, T., Taviani, M., 2016. Antarctic ice sheet sensitivity to atmospheric CO_2 variations in the early to mid-Miocene. Proc. Natl. Acad. Sci. USA 113, 3453–3458.
Macklin, M.G., Lewin, J., Woodward, J.C., 2012. The fluvial record of climate change. Philos. Trans. R. Soc. A 370, 2143–2172.
Marshall, N., Novak, V., Cibaj, I., Krijgsman, W., Renema, W., Young, J., Morley, R., Fraser, N., Limbong, A., 2015. Dating Borneo's Deltaic Deluge: middle Miocene progradation of the Mahakam Delta. Palaios 30, 7–25.
McClay, K., Dooley, T., Ferguson, A., Poblet, J., 2000. Tectonic evolution of the Sanga Sanga block, Mahakam delta, Kalimantan, Indonesia. AAPG Bull. 84, 765–786.
Meyers, S.R., 2014. Astrochron: an R package for astrochronology. https://cran.r-project.org/web/packages/astrochron/index.html.
Meyers, S.R., Sageman, B.B., 2007. Quantification of deep-time orbital forcing by average spectral misfit. Am. J. Sci. 307 (5), 773–792.
Meyers, S.R., Sageman, B.B., Arthur, M.A., 2012. Obliquity forcing of organic matter accumulation during oceanic anoxic event 2. Paleoceanography 27 (3), PA32.
Miall, A., 2014. Fluvial Depositional Systems. Springer International Publishing.
Miller, K., Kominz, M., Browning, J., Wright, J., Mountain, G., Katz, M., Sugarman, P., Cramer, B., Christie, B., Pekar, S., 2005. The Phanerozoic record of global sea-level change. Science 310, 1293–1298.
Mitchell, R.N., Bice, D.M., Montanari, A., Cleaveland, L.C., Christianson, K.T., Coccioni, R., Hinnov, L.A., 2008. Oceanic anoxic cycles? Orbital prelude to the Bonarelli Level (OAE 2). Earth Planet. Sci. Lett. 267, 1–16. http://dx.doi.org/10.1016/j.epsl.2007.11.026.
Morley, R., Decker, J., Morley, H., Smith, S., 2006. Development of high resolution biostratigraphic framework for Kutei Basin. In: Proceedings, Jakarta International Geosciences Conference and Exhibition, pp. 1–5. http://www.palynova.com/published/Jakarta06-PG-27.pdf.
Morley, R.J., Morley, H.P., 2011. Neogene climate history of the Makassar Straits, Indonesia. Geol. Soc. (Lond.) Spec. Publ. 355, 319–332.
Moss, S., Chambers, J., 1999. Tertiary facies architecture in the Kutai Basin, Kalimantan, Indonesia. J. Asian Earth Sci. 17, 157–181.
Nichols, G., 2009. Sedimentology and Stratigraphy, 2nd ed. Wiley–Blackwell.
Peeters, J., Busschers, F., Stouthamer, E., 2014. Fluvial evolution of the Rhine during the last interglacial–glacial cycle in the southern North Sea basin: a review and look forward. Quat. Int. 357, 176–188.
Rahim, K.J., Burr, W.S., Thomson, D.J., 2014. Applications of Multitaper Spectral Analysis to Nonstationary Data. PhD thesis. Queen's University. R package version 1.0–11.
Renema, W., Bellwood, D.R., Braga, J.C., Bromfield, K., Hall, R., Johnson, K.G., Lunt, P., Meyer, C.P., McMonagle, L.B., Morley, R.J., O'Dea, A., Todd, J.A., Wesselingh, F.P., Wilson, M., Pandolfi, J.M., 2008. Hopping hotspots: global shifts in marine biodiversity. Science 321, 654–657.
Replumaz, A., Tapponnier, P., 2003. Reconstruction of the deformed collision zone between India and Asia by backward motion of lithospheric blocks. J. Geophys. Res. 108, 1–24.
Saller, A.H., Noah, J.T., Ruzuar, A.P., Schneider, R., 2004. Linked lowstand delta to basin-floor Fan deposition, offshore Indonesia: an analog for deep-water reservoir systems. AAPG Bull. 88, 21–46.
Santodomingo, N., Novak, N., Pretiković, V., Marshall, N., Di Martino, E., Capelli, G., Rösler, A., Reich, S., Braga, J.C., Renema, W., Johnson, K., 2015. A diverse patch reef from turbid habitats in the middle Miocene (East Kalimantan, Indonesia). Palaios 30, 128–149.
Santodomingo, N., Renema, W., Johnson, K., 2016. Understanding the murky history of the Coral Triangle: Miocene corals and reef habitats in East Kalimantan (Indonesia). Coral Reefs 35, 765–781.
Shackleton, N.J., Crowhurst, S.J., Weedon, G.P., Laskar, J., 1999. Astronomical calibration of Oligocene–Miocene time. Philos. Trans. R. Soc. A 357, 1907–1929.
Spada, G., Bamber, J., Hurkmans, R., 2013. The gravitationally consistent sea-level fingerprint of future terrestrial ice loss. Geophys. Res. Lett. 40, 482–486.
Sykes, R., Cibaj, I., 2010. Peat biomass and early diagenetic controls on oil generation from Mahakam Delta Coal, Kutei Basin: preliminary study of coal from the Jalan Baru section near Samarinda. In: Proceedings From the Indonesian Petroleum Association Convention. May 2010.
Taner, M.T., 1992. Attributes Revisited. Technical Report. Rock Solid Images, Inc. http://www.rocksolidimages.com/attributes-revisited/.
Tian, S., Chen, Z., Huang, C., Gao, C., Zha, M., 2013. Astronomical dating of the middle Miocene Hanjiang formation in the Pearl river Mouth basin, South China Sea. Acta Geol. Sin. 87, 48–58.
Thomson, D.J., 1982. Spectrum estimation and harmonic analysis. Proc. IEEE 70, 1055–1096.
Valero, L., Huerta, P., Garcés, M., Armenteros, I., Beamud, E., Gómez-Paccard, M., 2015. Linking Sedimentation Rates and Large-Scale Architecture for Facies Prediction in Nonmarine Basins (Paleogene, Almazán Basin, Spain). Basin Research.
Wilson, M., 2005. Development of equatorial delta-front patch reef development during the Neogene, Borneo. J. Sediment. Res. 75, 116–134.
Witts, D., Davies, L., Morley, R., Anderson, L., 2015. Neogene deformation of East Kalimantan, a regional perspective. In: Proceedings From the Indonesian Petroleum Association Convention, May 2015.
Zeeden, C., Hilgen, F., Westerhold, T., Lourens, L., Röhl, U., Bickert, T., 2013. Revised Miocene splice, astronomical tuning and calcareous plankton biochronology of ODP Site 925 between 5 and 14.4 Ma. Palaeogeogr. Palaeoclimatol. Palaeoecol. 369, 430–451.
Zhu, Y., Bhattacharya, J.P., Li, W., Lapen, T.J., Jucha, B.R., Singer, B.S., 2012. Milankovitch-scale sequence statigraphy and stepped forced regressions of the Turonian Ferron Notom Deltaic Complex, South-Central Utah, USA. J. Sediment. Res. 82, 723–746.